



HAL
open science

Design-for-manufacturability of MEMS convective accelerometers through adaptive electrical calibration strategy

Ahmed Rekik, Florence Azaïs, Frédéric Mailly, Pascal Nouet

► **To cite this version:**

Ahmed Rekik, Florence Azaïs, Frédéric Mailly, Pascal Nouet. Design-for-manufacturability of MEMS convective accelerometers through adaptive electrical calibration strategy. LATW: Latin American Test Workshop, Apr 2012, Quito, Ecuador. 10.1109/LATW.2012.6261237 . lirmm-00803451

HAL Id: lirmm-00803451

<https://hal-lirmm.ccsd.cnrs.fr/lirmm-00803451v1>

Submitted on 21 Jan 2017

HAL is a multi-disciplinary open access archive for the deposit and dissemination of scientific research documents, whether they are published or not. The documents may come from teaching and research institutions in France or abroad, or from public or private research centers.

L'archive ouverte pluridisciplinaire **HAL**, est destinée au dépôt et à la diffusion de documents scientifiques de niveau recherche, publiés ou non, émanant des établissements d'enseignement et de recherche français ou étrangers, des laboratoires publics ou privés.

Design-for-manufacturability of MEMS convective accelerometers through adaptive electrical calibration strategy

A.A. Rekik^{1,2}, F. Azaïs¹, F. Mailly¹, P. Nouet¹

¹ LIRMM - CNRS/Univ. Montpellier 2 - 161 rue Ada, 34392 Montpellier, France

² ENIS - University of Sfax - Route Soukra, Cité Elhabib BP W 3052 Sfax, Tunisia

Abstract— In this paper, we explore the use of an adaptive electrical calibration strategy in the context of design-for-manufacturing for MEMS convective accelerometers. The calibration principle relies on the adjustment of the heater power level such that sensitivity is set to a given target value. The idea is to define multiple sensitivity targets in order to improve production yield and to insert a criterion on power consumption. Different device binning can then be achieved depending on test limit settings. Results obtained from Monte-Carlo simulation are presented to demonstrate potentialities of the technique.

Keywords— MEMS, convective accelerometer, test, calibration, design-for-manufacturing

I. INTRODUCTION

MEMS convective accelerometers are an interesting alternative to comb-drive accelerometers even if current market is largely devoted to the latter [1]. Their interest is twofold. On the one side, they can be fabricated in a CMOS technology with a single self-aligned additional etching [2]. This post-process called Front-Side Bulk Micromachining is one of the most popular in MEMS. On the other side, such accelerometers exhibit large dynamic range and huge safety range (they can support several thousands of g's without any damage).

Apart from the previous two advantages, we intend to demonstrate in this paper that convective accelerometers can be associated with design for manufacturing approaches to make them more appealing. Design for Manufacturability (DfM) generally includes Design for Test, Calibration, Reliability... often called DfX [3]. In our case, convective accelerometers already demonstrated their reliability so it is not necessary to work on their design to improve reliability. In some previous studies, we proposed techniques for test and calibration of such accelerometers using electrical-only stimuli [4-6]. This point is really important as the cost of these test procedures may drastically impact the final cost in the case of low-end products such as those used for consumer applications. In this paper, we propose to extend the previously proposed go/no-go scheme to a complete calibration and binning procedure.

The paper is organized as follow. In section II, the Device Under Test (DUT) is introduced together with a parametric fault model used to represent process scattering effects. In section III, electrical-only calibration procedure is described to introduce, in section IV, the adaptive electrical calibration strategy that allows binning on device sensitivity and power consumption. Finally, section V reports experimental results before conclusion.

II. DEVICE UNDER TEST OVERVIEW

A. Device description

The device under test is a convective accelerometer obtained by Front-Side Bulk Micromachining (FSBM) of a CMOS die. As illustrated in figure 1, three thin bridges composed of the CMOS process back-end layers (oxide, polysilicon, aluminum, and nitride) are suspended over a silicon etched cavity and polysilicon is used to realize temperature-sensitive resistors for heat generation (R_H) and temperature sensing (R_{D1}, R_{D2}).

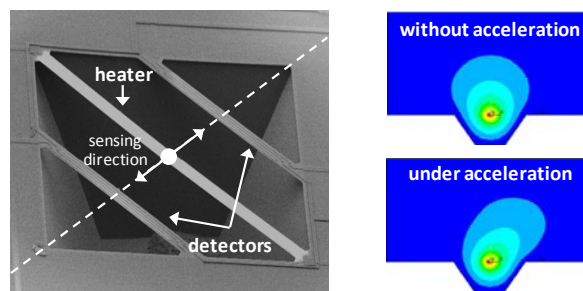


Figure 1. MEMS convective accelerometer

Sensor operating principle relies on heat transfer and more precisely on free convection of a hot bubble in a cavity. The hot bubble is created within the cavity by dissipating power in the heating resistor. In absence of acceleration, the temperature profiles around the heater are symmetrical and both detectors sense the same temperature. Acceleration applied along the sensitive axis causes disturbance of temperature profiles due to convection and a differential temperature appears between both detectors. This difference of temperature is then converted into a differential variation of resistance thanks to the Temperature Coefficient of Resistance (TCR) of polysilicon. Finally, a differential voltage is obtained as temperature sensors are arranged in a Wheatstone bridge with two reference resistors (R_{REF1}, R_{REF2}) located on the substrate. The so-obtained differential output voltage is directly proportional to applied acceleration and device sensitivity. For more details on sensor modeling, manufacturing and characterization please refer to previous works from some of the authors [2,7].

B. Parametric fault model

The behavioral model presented in [8] is used in this work to simulate parametric faults due to process scattering. More precisely, all electrical and geometrical model parameters will be altered to represent the effect of process scattering.

In particular, we consider a Gaussian distribution with $3\sigma=20\%$ for electrical resistances, i.e. heater resistance R_{H0} , detectors' resistances R_{Di0} , and reference resistances R_{REFi} . This distribution corresponds to typical uncertainties given by the foundry and is a global variation, i.e. it affects all resistances in the same amount. In addition, we consider a mismatch error with $3\sigma=2\%$ for detectors' resistances R_{Di0} and reference resistances R_{REFi} . We also consider a Gaussian distribution with $3\sigma=10\%$ for polysilicon temperature coefficient of resistance TCR as this parameter is quite sensitive to doping fluctuations.

Regarding geometrical parameters, we consider a Gaussian distribution with $3\sigma=2\mu\text{m}$ for the distance r_2 between the heater and the cavity boundary. Indeed, lateral dimensions are parameters that are rather well controlled during the manufacturing process and exhibit a low dispersion. In contrast, the cavity depth h_1 is a parameter that it is very sensitive to the etching post-process (etching solution composition, etching time and etching solution movements) and therefore very difficult to control. As we have no information from the foundry, we consider a random uniform variation of cavity depth h_1 between $50\mu\text{m}$ and $490\mu\text{m}$.

III. PREVIOUS WORK ON ELECTRICAL CALIBRATION

In a previous work [6], we developed an alternative electrical scheme that permits to calibrate the sensor sensitivity without the need of applying a calibrated acceleration. The basic principle consists in adjusting the power dissipated in the heating element so that the relative deviation of Wheatstone bridge equivalent impedance is set to a given target value corresponding to sensitivity nominal specification. A simple on-chip circuitry based on a pulse-modulated generator is integrated within the circuit to permit the adjustment of the power level through digital programming. As illustrated in figure 2, the generator is composed of an N-bit register to store the programming word, an N-bit maximal-length LFSR and an N-bit comparator. The comparator output controls two switches that bias the heating element to either V_{dd} or ground. As a result, the average power level dissipated in the heating element P_H is directly proportional to the programming word stored in the N-bit register. The fundamentals of the calibration technique are recalled in this section.

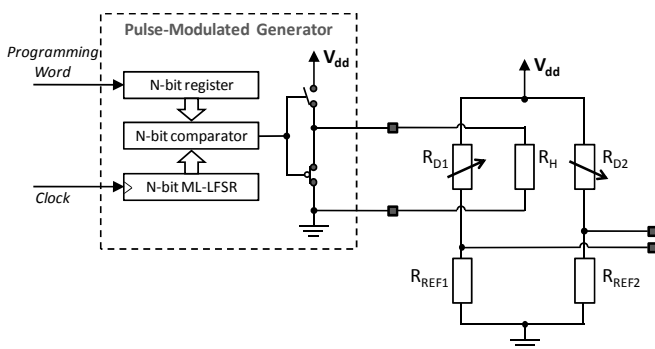


Figure 2. Schematic view of the device equipped with on-chip calibration facilities

The key parameter of the calibration technique is the relative deviation of Wheatstone bridge impedance due to power dissipation in the heating element. The evaluation of this

parameter only necessitates two simple static measurements of the current flowing through the Wheatstone bridge: (i) the current I_{W0} when no power is dissipated in the heating element ($Programming_Word = "00000"$) and (ii) the current I_W when a power P_H is dissipated in the heating element ($Programming_Word \neq "00000"$). The corresponding relative deviation of Wheatstone bridge impedance $\Delta R_{eq}/R_{eq0}$ is then computed with the following equation:

$$\frac{\Delta R_{eq}}{R_{eq0}} = \frac{I_W - I_{W0}}{I_{W0}} \quad (1)$$

The main interest of this parameter is that it presents a good correlation with device sensitivity. It can therefore be used to evaluate the device sensitivity without the need of applying a calibrated acceleration. As an illustration, figure 3 plots the relative deviation of Wheatstone bridge impedance for nominal heater power level $P_H=50\%$ versus the device sensitivity to 1g acceleration (obtained from Monte-Carlo simulations).

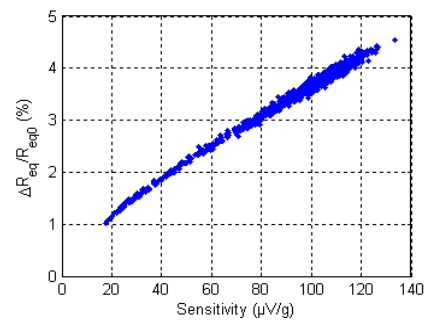


Figure 3. Relative deviation of Wheatstone bridge equivalent impedance ($\Delta R_{eq}/R_{eq0}$) vs. device sensitivity (S)

Then to act on the device sensitivity, the chosen approach was to adapt the power dissipated in the heating element. Indeed as depicted in figure 4, it exists a monotonic relationship between device sensitivity (S) and power dissipated in the heater (P_H), and therefore a possibility to perform calibration by playing on this electrical parameter. Such a solution is exploited in [9] to compensate for temperature variations in the silicon substrate and/or the local environment. In our case, the objective is to adjust the power dissipated in the heating element to compensate for process variation device susceptibility.

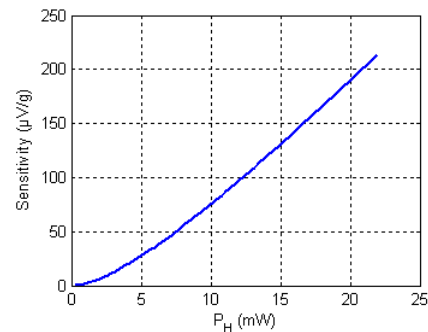


Figure 4. Device sensitivity (S) vs. heater power (P_H)

The proposed calibration strategy consists in adjusting the power dissipated in the heating element depending on the measurement of the relative deviation of Wheatstone bridge

impedance since this parameter presents good correlation with device sensitivity. More precisely, the idea is to adjust the heater power level so that the relative deviation of Wheatstone bridge impedance is set to a given target value $\Delta R_{eq}/R_{eq0}|_{target}$ corresponding to the nominal device sensitivity S_{spec} . The problem is that it is not possible to relate the relative deviation of Wheatstone bridge impedance and the heater power level with a unique relationship, but each device has a different curve which is not known a priori (see figure 5). In other words to reach the same target value $\Delta R_{eq}/R_{eq0}|_{target}$ for each individual device k , a different setting on the heater power level P_H^k has to be realized.

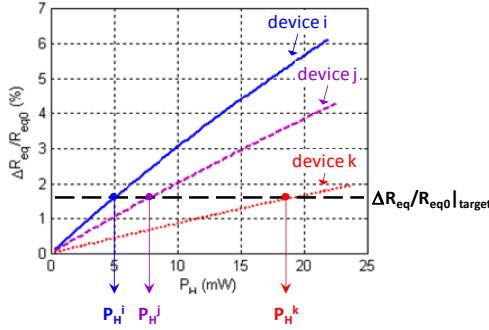


Figure 5. Relative deviation of Wheatstone bridge equivalent impedance ($\Delta R_{eq}/R_{eq0}$) vs. heater power level (P_H) for three different devices

To cope with this issue, we developed an iterative procedure that permits to search, for each individual device k , the appropriate power level P_H^k . More precisely at each iteration, the device is biased with the power level $P_H(i)$ determined in the previous iteration and the current $I_W(i)$ flowing through the Wheatstone bridge is measured in order to determine the corresponding relative deviation of Wheatstone bridge impedance $\Delta R_{eq}/R_{eq0}(i)$. Taking into account the target value $\Delta R_{eq}/R_{eq0}|_{target}$, the following value of the heater power level $P_H^k(i+1)$ is then determined from a linear interpolation/extrapolation between the two preceding measurements with:

$$P_H^k(i+1) = \frac{P_H^k(i) - P_H^k(i-1)}{\Delta R_{eq}/R_{eq0}^k(i) - \Delta R_{eq}/R_{eq0}^k(i-1)} * \Delta R_{eq}/R_{eq0}|_{target} + \frac{P_H^k(i) * \Delta R_{eq}/R_{eq0}^k(i-1) - P_H^k(i-1) * \Delta R_{eq}/R_{eq0}^k(i)}{\Delta R_{eq}/R_{eq0}^k(i-1) - \Delta R_{eq}/R_{eq0}^k(i)} \quad (2)$$

The electrical calibration flow is summarized in figure 6. The initial step of the procedure consists measuring the current flowing through the Wheatstone bridge at ambient temperature ($P_H(0)=0$) and under nominal power level condition ($P_H(1)=50\%$). From this, the relative deviation of Wheatstone bridge equivalent impedance $\Delta R_{eq}/R_{eq0}(1)$ can be computed and the iterative search begins. We actually determined that two iterations are sufficient to determine the appropriate heater power level, i.e. $P_H(3)$ is the final heater power level used for each device. In addition, an intermediate constraint was introduced at the end of the first iteration that reject devices for which the initial relative deviation of Wheatstone bridge equivalent impedance $\Delta R_{eq}/R_{eq0}(1)$ is below a predefined limit $\Delta R_{eq}/R_{eq0}|_{limit}$. Indeed these devices correspond to devices with a

very low sensitivity; taking into account that the maximum power level is limited to $(2^N-1)/2^N * P_{H,max}$, the possible increase in the power dissipated in the heater is not sufficient for these devices to compensate their poor sensitivity.

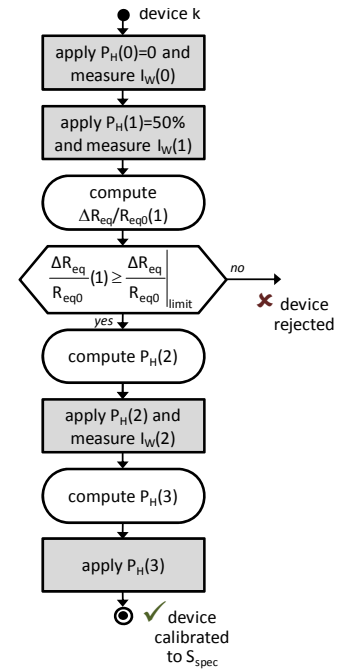


Figure 6. Electrical calibration flow

IV. ADAPTIVE ELECTRICAL CALIBRATION STRATEGY

An interesting feature of the calibration method is that it permits to adjust devices at different sensitivity values depending on the target value chosen for the relative deviation of Wheatstone bridge impedance. This flexibility can be exploited in the general context of design-for-manufacturability. In this section, we first present an adaptive version of the calibration procedure with multiple sensitivity targets in order to improve production yield. We then introduce a refinement of the procedure that permits to perform product binning taking into account both sensitivity and power consumption specifications.

A. Binning on device sensitivity

The objective is to exploit the flexibility offered by the calibration method in order to improve the production yield. Indeed a number of devices are rejected by the calibration procedure presented in the previous section because they present a poor initial sensitivity under nominal heater power level. The idea is, instead of rejecting these devices, to calibrate them to a lower sensitivity specification.

To illustrate this strategy, let us consider 2 different values of sensitivity specification S_{spec1} and S_{spec2} (with $S_{spec1} > S_{spec2}$), corresponding to 2 different target values $\Delta R_{eq}/R_{eq0}|_{target1}$ and $\Delta R_{eq}/R_{eq0}|_{target2}$. The related adaptive calibration flow is depicted in figure 7, which bins devices in three categories:

- Category 1: devices that exhibits an initial relative deviation of Wheatstone bridge impedance $\Delta R_{eq}/R_{eq0}(1)$ higher than $\Delta R_{eq}/R_{eq0}|_{limit1}$. These devices

go to the calibration procedure using $\Delta R_{eq}/R_{eq0}|_{target1}$. Their sensitivities would be centered on S_{spec1} ; they correspond to accepted devices.

- Category 2: devices that exhibits an initial relative deviation of Wheatstone bridge impedance $\Delta R_{eq}/R_{eq0}(1)$ lower than $\Delta R_{eq}/R_{eq0}|_{limit1}$ but higher than $\Delta R_{eq}/R_{eq0}|_{limit2}$. These devices go to the calibration procedure using $\Delta R_{eq}/R_{eq0}|_{target2}$; their sensitivities would be centered on S_{spec2} ; they correspond to accepted devices.
- Category 3: devices that exhibits an initial relative deviation of Wheatstone bridge impedance $\Delta R_{eq}/R_{eq0}(1)$ lower than $\Delta R_{eq}/R_{eq0}|_{limit2}$. These devices are rejected by the procedure.

Obviously, the number of categories can be freely chosen depending on the application. The test limit values have then to be adapted for each category.

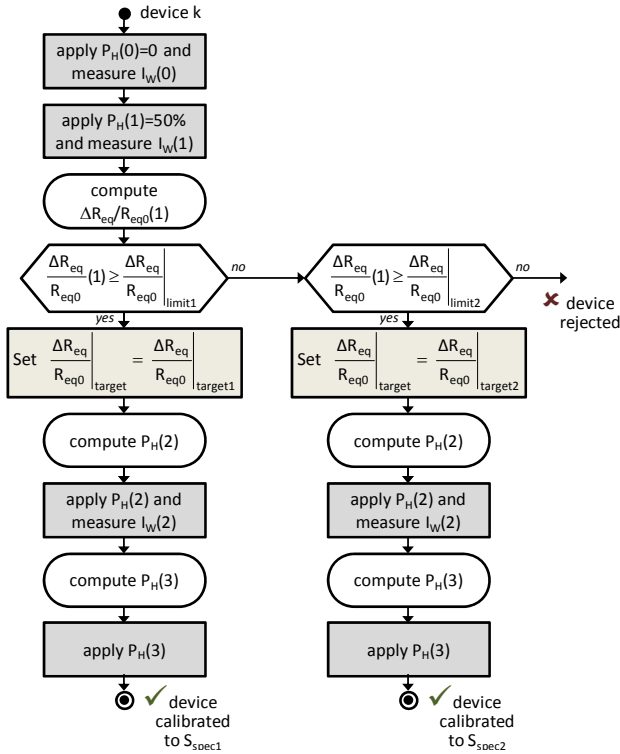


Figure 7. Adaptive procedure for product binning with focus on device sensitivity

B. Binning on both device sensitivity and power consumption

Depending on the application, power consumption may be another important parameter in addition to sensitivity. Since the proposed calibration procedure is based on the adjustment of the heater power level, it is more than probable that for some circuits (especially circuits with very poor initial sensitivity), power consumption significantly increases after calibration.

In this context, a refinement of the calibration procedure consists in including an extra criterion on power consumption in addition to sensitivity calibration, as illustrated in the flow diagram of figure 8. In this procedure, each device is first directed for calibration towards the highest possible sensitivity

specification according the measurement of its initial relative deviation of Wheatstone bridge impedance, and then possibly redirected to lower sensitivity specification if power consumption constraints are not satisfied (we assume that most of the power consumption comes from the power dissipated in the heating element).

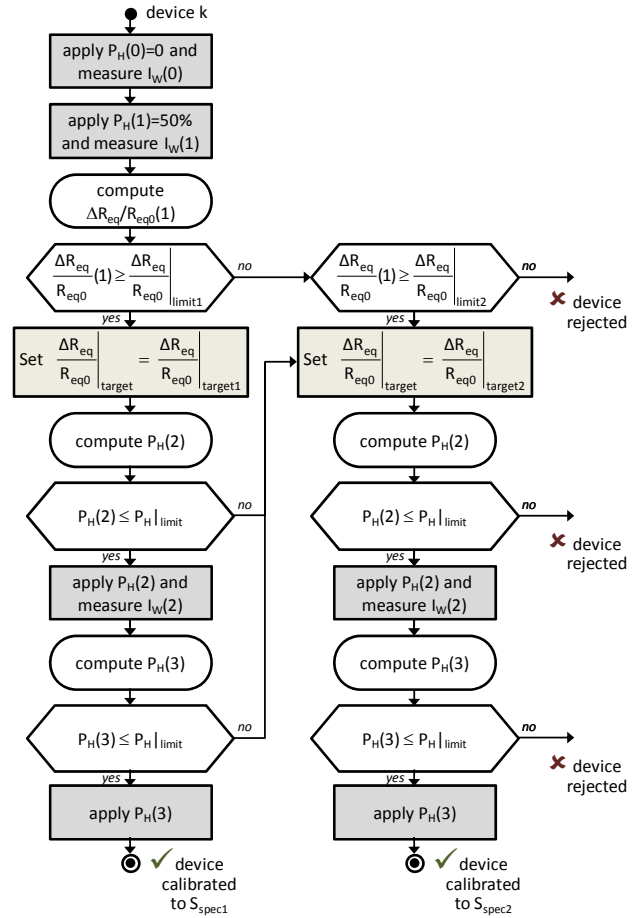


Figure 8. Adaptive procedure for product binning with focus on both device sensitivity and power consumption

V. RESULTS

A number of simulations have been carried in order to evaluate the performances of the proposed adaptive calibration strategy. A population of 1,000 devices generated through Monte-Carlo simulations has been considered using the parametric fault model described in section II.

First, we have applied the original calibration procedure with a single sensitivity target. The objective was to calibrate devices to a nominal sensitivity $S_{spec} = 100\mu V/g$, which corresponds to a target value $\Delta R_{eq}/R_{eq0}|_{target} = 3.657\%$ (determined from a simulation with all parameters at typical value). Results are illustrated in figure 9, which gives the distribution of device sensitivity before and after calibration. Initially, device sensitivity exhibits a rather large dispersion and only 541 out of 1,000 devices are within $\pm 10\%$ nominal sensitivity specification. Applying the calibration procedure, 67 devices are actually rejected (with $\Delta R_{eq}/R_{eq0}|_{limit} = 1.87\%$), but the dispersion on device sensitivity is significantly reduced

and the distribution is well centered on the desired specification. This calibration procedure therefore permits to increase the production yield from 54.1% to 93.3%.

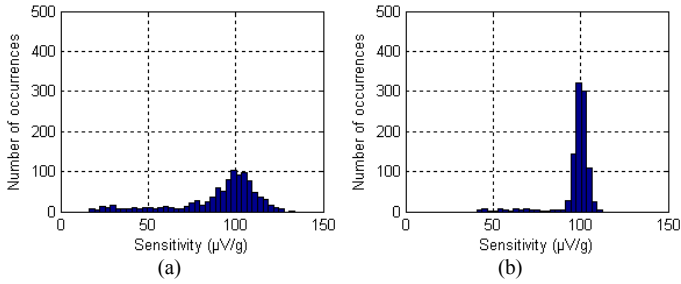


Figure 9. Distribution of device sensitivity before (a) and after (b) calibration with single sensitivity target.

Then, we have applied the adaptive calibration strategy considering multiple sensitivity targets. In this experiment, we consider three different values of sensitivity specification $S_{spec1} = 100\mu\text{V/g}$, $S_{spec2} = 75\mu\text{V/g}$ and $S_{spec3} = 50\mu\text{V/g}$, corresponding to three different target values $\Delta R_{eq}/R_{eq0}|_{target1} = 3.657\%$, $\Delta R_{eq}/R_{eq0}|_{target2} = 2.937\%$ and $\Delta R_{eq}/R_{eq0}|_{target3} = 2.208\%$. Devices are therefore binned in four categories:

- Category 1: devices that exhibits an initial relative deviation of Wheatstone bridge impedance $\Delta R_{eq}/R_{eq0}(1)$ higher than $\Delta R_{eq}/R_{eq0}|_{limit1} = 1.87\%$. These devices go to the calibration procedure using $\Delta R_{eq}/R_{eq0}|_{target1}$. Their sensitivities would be centered on S_{spec1} ; they correspond to accepted devices.
- Category 2: devices that exhibits an initial relative deviation of Wheatstone bridge impedance $\Delta R_{eq}/R_{eq0}(1)$ lower than $\Delta R_{eq}/R_{eq0}|_{limit1} = 1.87\%$ but higher than $\Delta R_{eq}/R_{eq0}|_{limit2} = 1.52\%$. These devices go to the calibration procedure using $\Delta R_{eq}/R_{eq0}|_{target2}$; their sensitivities would be centered on S_{spec2} ; they correspond to accepted devices.
- Category 3: devices that exhibits an initial relative deviation of Wheatstone bridge impedance $\Delta R_{eq}/R_{eq0}(1)$ lower than $\Delta R_{eq}/R_{eq0}|_{limit2} = 1.52\%$ but higher than $\Delta R_{eq}/R_{eq0}|_{limit3} = 1.11\%$. These devices go to the calibration procedure using $\Delta R_{eq}/R_{eq0}|_{target3}$; their sensitivities would be centered on S_{spec3} ; they correspond to accepted devices.
- Category 4: devices that exhibits an initial relative deviation of Wheatstone bridge impedance $\Delta R_{eq}/R_{eq0}(1)$ lower than $\Delta R_{eq}/R_{eq0}|_{limit3} = 1.11\%$. These devices are rejected by the procedure.

On this example, the test limit values have been set so that they favor the categories of highest sensitivity specification. Results are illustrated in figure 10, which gives the distribution of device sensitivity after application of the calibration procedure. As expected, the sensitivity histogram reveals three non-overlapping distributions centered on the targeted sensitivities. In this case, only 5 devices are rejected by the calibration procedure, which corresponds to a theoretical production yield of 99.5%. The effectiveness of the adaptive calibration strategy to improve production yield is therefore

clearly demonstrated. However, it should be noted that the procedure is not able to guarantee a calibration success rate of 100%. In this experiment, there are 15 accepted devices for which sensitivity is close to the specification, but not exactly within $\pm 10\%$ range. This corresponds to a test escape of 1.5%. The actual production yield is therefore 98% after calibration.

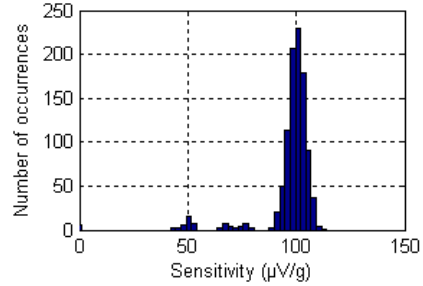


Figure 10. Distribution of device sensitivity after calibration with multiple sensitivity target.

Because the calibration procedure is based on the adjustment of the heater power level, the device power consumption is significantly affected. To illustrate this point, figure 11 reports the heating power distribution before and after calibration. Before calibration, all devices have their heating power in a range of $\pm 25\%$ of the typical heating power value ($P_{Htyp} = 12.2\text{mW}$); after calibration, only 80.2% of calibrated devices have their heating power in a range of $P_{Htyp} + 25\%$. Consequently, if power consumption is also a specification to be satisfied, it is clear that some calibrated devices should be rejected, therefore reducing production yield. On this example, rejecting all devices with a heating power that exceeds $P_{Htyp} + 25\%$ results in a global production yield of 80.2%.

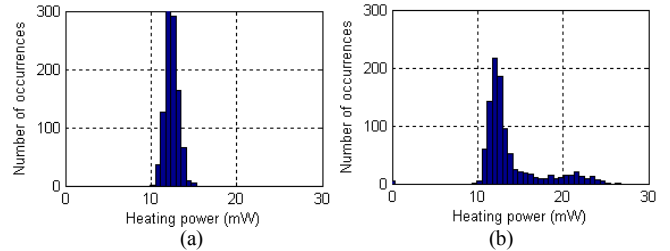


Figure 11. Distribution of heating power before (a) and after (b) calibration.

The objective of the adaptive calibration procedure introduced in section IV.B is to optimize product binning when specifications on both device sensitivity and power consumption have to be satisfied. In this case, an additional constraint on the heating power $P_{H|limit}$ is inserted in the calibration procedure. Figure 12 compares the distribution of device sensitivity and heating power achieved after calibration, without and with this additional criterion inserted in the flow ($P_{H|limit} = P_{Htyp} \pm 25\%$ in this experiment). With the first approach, 198 devices are rejected whereas only 70 devices are rejected with the second approach. The production yield therefore improves from 80.2% to 93%. Moreover, an interesting consequence of the insertion of the additional constraint on heating power is that the calibration success rate is increased. In this experiment, there is only one accepted device for which sensitivity is close to the specification, but not exactly within $\pm 10\%$ range.

VI. CONCLUSIONS

In the context of design-for-manufacturing of MEMS convective accelerometers, we have proposed an adaptive calibration strategy that permits product binning based on both sensitivity and power consumption performances. The idea is to adjust devices at different sensitivity values using different target values for the relative deviation of Wheatstone bridge impedance. The target value applied for each device depends on both its initial sensitivity and power consumption constraint. Results have shown the efficiency of the technique that permits to improve initial production yield ranging from 50% to 65% up to production yield ranging from 91% to 98% depending on power consumption constraint. Moreover it is a low-cost procedure since it requires only electrical measurements.

REFERENCES

- [1] H. Xie et al, Accelerometers, chap 2.05 of Comprehensive Microsystems, ISBN: 978-0-444-52190-3, pp. 135-180, 2008.
- [2] A. Chaoi et al., Experimental and finite-element study of convective accelerometer on CMOS, Sensors and Actuators A 132/1, pp. 78-84, 2006.
- [3] A Richardson, Design for Manufacture Challenges in MEMS enabled Micro & Nano Systems, ESSCIRC tutorial, 2008.
- [4] A.A. Rekik et al., Investigations on Electrical-only Test Setup for MEMS Convective Accelerometer, Proc. IEEE Int'l Conference on Signals, Circuits and Systems (SCS'09), 2009.
- [5] A.A. Rekik et al., An electrical test method for MEMS convective accelerometers: development and evaluation, Proc. Design Automation & Test in Europe (DATE'11), 2011.
- [6] A.A. Rekik et al., A MEMS convective accelerometer equipped with on-chip facilities for sensitivity electrical calibration, Proc. IEEE Int'l Mixed-Signals, Sensors & Systems Test Workshop (IMS3TW'11), 2011.
- [7] O. Leman et al., Modeling and system-level simulation of a CMOS convective accelerometer, Solid-State Electronics, Volume 51, Issues 11-12, pp. 1609-1617, 2007.
- [8] A.A. Rekik et al., Modeling the influence of etching defects on the sensitivity of MEMS convective accelerometers, Proc. IEEE Int'l Mixed-Signals, Sensors and Systems Test Workshop (IMS3TW'10), 2010.
- [9] Y. Zhao et al., Thermal convection accelerometer with closed-loop heater control, US Patent 6,795,752 B1, Sept. 2004

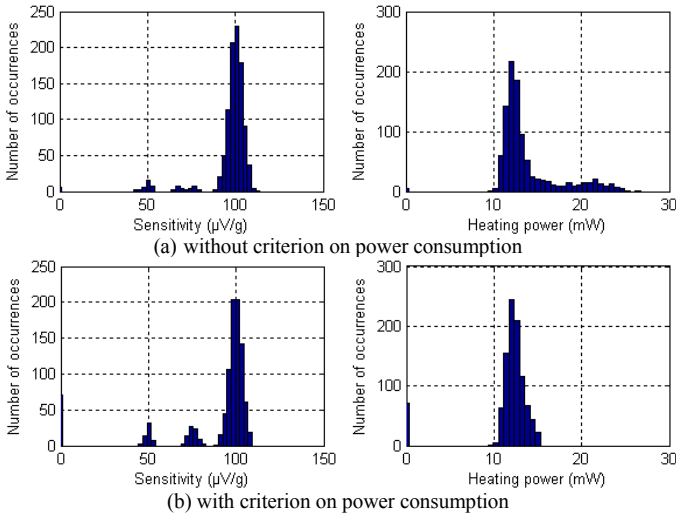


Figure 12. Distribution of device sensitivity and heating power after adaptive calibration.

More generally to analyze the performance of the proposed adaptive calibration strategy, we have compared the repartition of devices in each category (considering both device sensitivity and power consumption) before and after application of the calibration procedure. Results are summarized in figure 13, for different values of the constraint on the heating power $P_{H|limit}$. In all cases, the proposed adaptive calibration strategy permits to significantly improve the production yield. When considering only sensitivity, production yield theoretically increases from 65.4% to 99.5%. However as already mentioned, there are some test escapes that lead to a slightly lower production yield at 98%. Interestingly when considering both sensitivity and power consumption, the number of test escapes falls to 1 or 2, resulting in an actual production yield extremely close to the theoretical one. Besides, it can be noticed that the proposed strategy is able to efficiently manage different constraints on power consumption: even with a very tight constraint at $P_{Htyp}+10\%$; the actual production yield after calibration is higher than 90% while only about 50% of the devices are initially within specification.

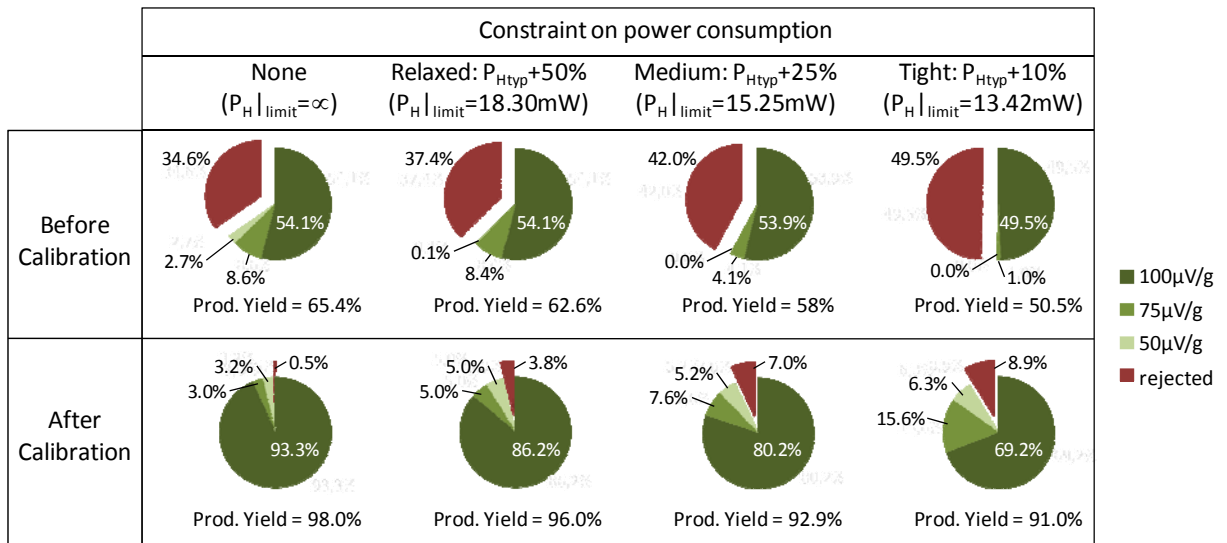


Figure 13. Distribution of device sensitivity after adaptive calibration for different values of $P_{H|limit}$.